GLIA

GLIA 60:175–188 (2012)

Neuronal Activity Regulates Glutamate Transporter Dynamics in Developing Astrocytes

ADRIENNE M. BENEDIKTSSON,[1] GLEN S. MARRS,[1] JIAN CHENG TU,[2] PAUL F. WORLEY,[2] JEFFREY D. ROTHSTEIN,[2,3] DWIGHT E. BERGLES,[2] AND MICHAEL E. DAILEY[1,4]*

[1]*Program in Neuroscience, University of Iowa, Iowa City, Iowa*
[2]*Solomon H. Snyder Department of Neuroscience, Johns Hopkins University Medical School, Baltimore, Maryland*
[3]*Department of Neurology, Johns Hopkins University Medical School, Baltimore, Maryland*
[4]*Department of Biology, University of Iowa, Iowa City, Iowa*

KEY WORDS
astrocyte; GLT-1; EAAT2; biolistics; time-lapse; activity

ABSTRACT
Glutamate transporters (GluTs) maintain a low ambient level of glutamate in the central nervous system (CNS) and shape the activation of glutamate receptors at synapses. Nevertheless, the mechanisms that regulate the trafficking and localization of transporters near sites of glutamate release are poorly understood. Here, we examined the subcellular distribution and dynamic remodeling of the predominant GluT GLT-1 (excitatory amino acid transporter 2, EAAT2) in developing hippocampal astrocytes. Immunolabeling revealed that endogenous GLT-1 is concentrated into discrete clusters along branches of developing astrocytes that were apposed preferentially to synapsin-1 positive synapses. Green fluorescent protein (GFP)-GLT-1 fusion proteins expressed in astrocytes also formed distinct clusters that lined the edges of astrocyte processes, as well as the tips of filopodia and spine-like structures. Time-lapse three-dimensional confocal imaging in tissue slices revealed that GFP-GLT-1 clusters were dynamically remodeled on a timescale of minutes. Some transporter clusters moved within developing astrocyte branches as filopodia extended and retracted, while others maintained stable positions at the tips of spine-like structures. Blockade of neuronal activity with tetrodotoxin reduced both the density and perisynaptic localization of GLT-1 clusters. Conversely, enhancement of neuronal activity increased the size of GLT-1 clusters and their proximity to synapses. Together, these findings indicate that neuronal activity influences both the organization of GluTs in developing astrocyte membranes and their position relative to synapses.

INTRODUCTION

Surface glutamate transporters (GluTs) prevent the accumulation of extracellular glutamate, preserve the responsiveness of glutamate receptors (GluRs), and prevent glutamate-induced excitotoxicity (Huang and Bergles, 2004; Tzingounis and Wadiche, 2007). Moreover, normal brain development depends on GluT function (Matsugami et al., 2006). Of the known GluTs in the CNS, GLT-1 (EAAT2) is the most abundant and is responsible for the majority of glutamate uptake in the forebrain (Danbolt, 2001; Rothstein et al., 1994; Tanaka et al., 1997). In the postnatal brain, GLT-1 is highly expressed by astrocytes (Danbolt, 2001; Rothstein et al., 1994) which extend processes near excitatory synapses (Kosaka and Hama, 1986; Spacek, 1985; Ventura and Harris, 1999), thereby placing GluTs near sites of neurotransmitter release. Retraction of perisynaptic astrocytic processes prolongs synaptic glutamate transients and enhances activation of receptors (Iino et al., 2001; Oliet et al., 2001), presumably by removing GluTs. By clearing glutamate that diffuses out of the synaptic cleft, GLT-1 regulates the amount of glutamate available to bind to receptors (Huang et al., 2004), particularly metabotropic receptors that reach their highest density in perisynaptic domains. However, the factors that influence the density and distribution of GLT-1 in astrocytes are poorly understood.

GLT-1 expression is increased when astrocytes are cultured with neurons, and conversely, astrocytes cultured without neurons often cease to express GLT-1 (Perego et al., 2000; Poitry-Yamate et al., 2002; Swanson et al., 1997). The density of GLT-1 *in situ* varies among astrocytes in different brain regions (Regan et al., 2007) and over the surface of individual cells, with highest densities found in membranes adjacent to neurons (Chaudhry et al., 1995). Furthermore, GLT-1 expression is reduced when synapses are lost following removal of glutamatergic afferents (Ginsberg et al., 1995, 1996; Yang et al., 2009) or through disease (Rothstein et al., 1995), while enhancing synaptic activity increases GLT-1 expression (Genoud et al., 2006). These results suggest that GLT-1 expression is regulated by neurons to ensure sufficient local uptake capacity.

GluTs operate independently within homotrimeric assemblies (Leary et al., 2007; Yernool et al., 2004) that

Additional Supporting Information may be found in the online version of this article.

Grant sponsor: NIH; Grant numbers: NS43468 (M.E.D.), NS44261 and MH084020 (D.E.B. and P.F.W.); Grant sponsors: Nellie Ball Trust (A.M.B. and M.E.D.); American Heart Association predoctoral fellowship (A.M.B.).

A. M. Benediktsson is currently at Department of Chemical and Biological Sciences, Mt. Royal University, Calgary, Alberta, Canada

G. S. Marrs is currently at Center for Neuroscience, West Virginia University School of Medicine, Morgantown, West Virginia, USA

J.C. Tu is currently at Department of Clinical Laboratory Medicine, Zhongnan Hospital, Wuhan University, Wuhan, China.

*Correspondence to: Michael E. Dailey, Department of Biology, University of Iowa, Iowa City, IA 52242. E-mail: michael-e-dailey@uiowa.edu

Received 25 March 2011; Accepted 2 September 2011

DOI 10.1002/glia.21249

Published online 2 November 2011 in Wiley Online Library (wileyonlinelibrary.com).

aggregate within cholesterol-rich lipid rafts at the cell surface (Butchbach et al., 2004; Sullivan et al., 2004). GLT-1 rich microdomains are found in cultured glioma cells virally induced to over-express GLT-1 (Zhou and Sutherland, 2004) and can be enhanced in astrocytes by exposure to glutamate (Poitry-Yamate et al., 2002). However, little is known about the distribution and dynamics of these clusters *in situ* or whether they are affected by neuronal activity.

Here, we defined the spatial pattern of GLT-1 *in situ* using organotypic hippocampal slice cultures, in which astrocytes develop a complex morphology and intimate relationships with other glia and neurons (Benediktsson et al., 2005; Dani et al., 1992; Derouiche et al., 1993). Our results revealed that GLT-1 clusters undergo rapid remodeling, and that changes in neuronal activity regulate the size and density of GLT-1 clusters as well as their apposition to synapses in developing brain tissues.

MATERIALS AND METHODS

Organotypic Tissue Slice Cultures

Organotypic hippocampal slice cultures were prepared as described previously (Benediktsson et al., 2005; Stoppini et al., 1991). Briefly, postnatal day (P) 5 to P7 Sprague Dawley rat pups were killed by swift decapitation, in accordance with institutional guidelines and as approved by the animal care and use committee. Brains were placed in cold (4°C) Hanks-balanced salt solution (HBSS; Gibco) supplemented with dextrose (6 mg/mL). Hemispheres were separated and hippocampi were isolated and cut into 300 μm thick transverse sections using a manual tissue chopper (Stoelting). Slices were placed onto Falcon polyethylene terephthalate-etched membrane culture inserts perforated with 1-μm pores (BD Biosciences). Slices were maintained in filter culture media (FCM) containing: 25% HBSS, 50% minimum essential medium (MEM), 25% heat-inactivated horse serum (HS), 2 mM glutamine, 0.044% $NaHCO_3$, and 10 U/mL penicillin–streptomycin. Tissues were cultured in a 5% CO_2 humidified incubator (36°C) for 2–14 days before use. Media was exchanged every 2 days.

Immunohistochemistry

Immunohistochemistry was performed as described previously (Benediktsson et al., 2005). Briefly, acutely isolated tissue slices (300 μm thick), or cultured slices on membrane inserts, were placed in warm culture media containing 4% paraformaldehyde for 15 min at room temperature. Tissues were rinsed in 0.01 M phosphate buffered saline (PBS), extracted overnight with 1% Triton-X, blocked sequentially in 50 mM NH_4Cl and 20% HS (30 min each), rinsed with PBS containing 1% HS (PBS+HS), and incubated for 10–16 h (4°C) in primary antibodies at the indicated dilutions: anti-GFAP mouse monoclonal (Sigma, catalog #G3893), 1:500; anti-GLT-1 rabbit polyclonal (Rothstein et al., 1994), 1:500; anti-GLT-1 guinea pig polyclonal (Chemicon, AB1783), 1:10,000; anti-synapsin-1 rabbit polyclonal (Invitrogen), 1:200; anti-GFP mouse monoclonal (Sigma, G6539), 1:500. Tissue slices were rinsed (3 × 15 min) with PBS+HS, then incubated 10–16 h (4°C) in Alexa-Fluor-488 or -568 conjugated secondary antibodies (Invitrogen), diluted 1:300 in PBS+HS, before final rinses and mounting.

Plasmid Construction and Characterization of GFP-GLT-1

Two different plasmids were used: a red fluorescent protein (DsRed2; Clontech) and a full length GLT-1 fused to GFP (GFP-GLT-1). To construct GFP-GLT-1, GFP was fused to the N-terminus of GLT-1 by inserting it in frame into the pEGFP-C3 vector (Clontech) between SalI and BamH1 restriction sites. For both plasmids, transcription was driven by a cytomegalovirus promoter. Plasmids for transfection were purified using a Plasmid Maxi Kit (Qiagen). Optimal DNA concentrations for gene gun bullets were between 0.9 and 1.5 μg/μL. The ability of the GFP-GLT-1 fusion protein to support glutamate uptake was evaluated after transient transfection of plasmid into HEK cells, as described (Davis et al., 1998). Cells were incubated with 1, 5, 10, 50, or 500 μM ^{3}[H]-L-glutamate at 37°C for 4 min, washed with PBS, dissolved in 0.1 N NaOH, and the radioactivity present in a 500-μL sample was measured with a scintillation counter. GFP-GLT-1 supported saturable, Na^+-dependent uptake of glutamate with a K_m = 35 μM, comparable to that exhibited by wild-type GLT-1 (Tan et al., 1999).

Preparation of cDNA Carriers and Biolistic Transfection in Hippocampal Tissue Slices

Biolistic transfection was performed using a Helios gene gun (Bio-Rad) as described in detail previously (Benediktsson et al., 2005; Marrs et al., 2001). Colloidal gold particles (1.0 μm diameter) were used as the plasmid carrier. DNA was added to gold to obtain the optimal ratio of DNA:gold, referred to as the DNA loading ratio [DLR = (concentration of DNA × volume used)/weight of gold]. Typically, a DLR of 2.0 was used, although somewhat higher transfection rates and expression levels could be achieved with a DLR up to 6.0. To make double bullets containing two different plasmids, the optimal DLR ratio was 1:3 for GFP-GLT-1:DsRed2. Gene gun "bullets" were prepared using a Bio-Rad tubing prep station. For biolistic transfection, the gene gun was shot from a distance of 1–2 cm at a pressure of 80–100 psi. Cultures were transfected 1–12 days after slicing and returned to the CO_2 incubator. Typically, slices were imaged 24–48 h after transfection.

Treatment of Organotypic Tissue Slices With Toxins

Slice cultures were exposed to one of three conditions: (1) control slices were cultured in FCM alone for 7 days (CTL); (2) slices were cultured for 7 days in 0.2 μM

tetrodotoxin (TTX; RBI) diluted in FCM (FCM+TTX); (3) slices were cultured for 6 days in FCM, then switched to 10 μM SR-95531 (gabazine, GBZ; Sigma) in FCM (FCM+GBZ) for 24 h before imaging. All media was exchanged every 48 h. Although GBZ treatment induces persisting patterns of enhanced network activity in slice cultures, this does not cause detectable cell death or other obvious features of pathology (Zha et al., 2005) presumably because developing hippocampal tissues are resistant to seizure-induced cell death (Haas et al., 2001).

Confocal Imaging and Image Processing

Images were captured using a Leica TCS NT scanning laser confocal microscope (inverted) equipped with Argon (Ar; 488 nm), Krypton (Kr; 568 nm), and Helium-Neon (He–Ne; 633 nm) lasers, or a Leica SP2 AOBS confocal system equipped with Ar, green He–Ne (543 nm), orange He–Ne (594 nm), and red He–Ne (633 nm) lasers. GFP-fusion proteins were visualized using the 488-nm Ar laser line and a fluorescein-like filter set, and DsRed2 was imaged using Ar or Kr laser excitation and a rhodamine-like filter set.

For three-dimensional reconstruction of cells in fixed tissue slices, stacks of 20–80 optical sections were taken (0.4–1.0 μm *z*-step intervals) using a 20×/0.7 Plan Apo or 63×/1.2 water Plan Apo lens. Two-dimensional (2D) projection images were generated in Image (Scion) or ImageJ (Wayne Rasband, NIH) using a maximum brightness operation.

Data Analysis

To assess localization of synapsin-1 with either GLT-1 immunopuncta or GFP-GLT-1, confocal image stacks representing 10–40 μm deep tissue volumes were displayed as 2D projection images using the Leica Confocal Software. Then 2-μm circular regions of interest (ROIs) were drawn around randomly selected GLT-1 clusters (blind to the synapsin-1 channel). After a cluster was selected, intensity values within the ROIs were calculated at each focal plane through the stack for both fluorescent channels, and peak intensities of both GLT-1 clusters and synapsin-1 immunopuncta were plotted through the *z*-stack of images. The GLT-1 cluster was scored as "apposed" if the peak intensity of the synapsin-1 channel was within 1 μm on either side of the peak intensity of the GLT-1 channel (in the z dimension). For GFP-GLT-1, an equal number of 2 μm diameter circles were randomly placed along regions of astrocytic processes where there were no obvious GLT-1 clusters. These ROIs were analyzed for apposition in three dimensions, as above. The statistical significance between "off-cluster" and "on-cluster" apposition to synapses was calculated using a Student's *t*-test. The statistical significance between treatment groups was first calculated using ANOVA, followed by a post hoc *t*-test.

To define GLT-1 cluster density, individual *z*-sections were thresholded to determine 2D-cell surface area, then the initial threshold level was doubled to capture bright clusters but not background fluorescence. Particle analysis was performed with a minimum of 1 pixel. By defining clusters as fluorescent regions at least 2× greater than the intensity of the diffuse membrane fluorescence, our analysis normalizes for any differences in expression levels between cells or treatment conditions. Where large suprathreshold areas appeared to be composed of overlapping clusters, a manual count was performed, comparing the thresholded and raw images.

All analyses were performed blind to condition. ANOVAs were calculated for each data set and then Post hoc Student's *t*-tests were performed for individual sets (TTX, GBZ, and CTL).

Time-Lapse Imaging

For time-lapse recordings, slice cultures were mounted in a closed chamber containing 4-(2-Hydroxyethyl)piperazine-1-ethanesulfonic acid, HEPES)-buffered culture media (500 μL), as described previously (Benediktsson et al., 2005; Dailey et al., 2011). The chamber was maintained at 35°C by warm, forced air, and media was exchanged every 2–3 h. The chamber medium lacked phenol red and contained antioxidant (25mM ascorbate) to scavange reactive oxygen species that may contribute to photodynamic damage (Dailey et al., 2006). To capture changes in astrocyte structure, stacks of 6–20 optical sections (512 × 512 pixel array) were collected at 1–6 min intervals. In most cases, image stacks were collected at 4–6 min intervals for several hours. In some brief (<1 h) time-lapse experiments, images were collected at 1 min intervals to capture rapid events with greater time resolution. To resolve fine details of astrocytic processes, a 63× lens was used with 1.5–3.5 additional electronic zoom. The *z*-step size between optical sections was usually ~ 0.8 μm (range 0.5–1.0 μm). Stacks of images were collected in the *z*-dimension in such a way that they were partially overlapping so that, within the volume of tissue imaged, structures did not get lost between individual images. Laser illumination was attenuated to a minimal level (10–20%) using an acousto-optical tunable filter, and the detector pinhole was opened (two airy units) to improve light collection. The continuously variable barrier filters on the Leica SP2 AOBS confocal were adjusted to maximize signal detection. Live cells coexpressing GFP and DsRed2 were illuminated at a single wavelength (488 nm) and detected simultaneously in two channels to reduce the light load. For improved signal-to-noise ratio, two to three scans were averaged at each optical section. At the beginning of each imaging session, detector gain and offset were adjusted so that the most intense fluorescence was just below detector saturation and the background (nonfluorescent) signal was just above the detection floor. Under these conditions, time-lapse recordings of healthy astrocytes were performed for 3–10 h without evidence of photobleaching or phototoxicity, such as blebbing or changes in cell activity (Dailey et al., 2011). Projection images were filtered (Gaussian blur in Adobe Photoshop) to reduce noise, and for a given

time series, all images were adjusted identically for brightness and contrast. To correct for any drift in the XY plane, projection images in time-lapse sequences were subjected to an automatic subpixel registration algorithm for rigid body motion (Thévenaz et al., 1998) using the StackReg plugin in ImageJ.

RESULTS

Astrocytes maintained in dissociated cell culture lose their highly ramified appearance, and over time cease to express GLT-1 (Danbolt, 2001), suggesting that they revert to a more immature phenotype. In contrast, many astrocytes within organotypic slice cultures retain a complex morphology, and extend numerous processes with fine lamellar extensions that contact neurons, synapses, and other astrocytes (Benediktsson et al., 2005; Dani et al., 1992; Derouiche et al., 1993). The preservation of a dense cytoarchitecture in organotypic slices offers advantages for manipulating astrocytes and assessing their responses to changes in neuronal activity. To study the subcellular distribution and dynamic remodeling of astroglial GluTs in developing hippocampal slices, we used immunocytochemistry to label endogenous GLT-1 and particle-mediated gene transfer to express a GFP-GLT-1 fusion protein in transfected astrocytes.

Endogenous GLT-1 Exhibits a Punctate Distribution in Developing Hippocampus

Astrocytes begin to express GLT-1 prenatally (Shibata et al., 1996), and in the forebrain levels of this transporter steadily increase during the first three postnatal weeks (Furuta et al., 1997). Immunolabeling for GLT-1 has revealed dense labeling of the neuropil, particularly within synaptic layers of "stratum radiatum" (SR) and "lacunosum-moleculare" of area CA1, in both the developing and adult hippocampus (Furuta et al., 1997; Williams et al., 2005). We used antibodies to determine if GLT-1 is distributed similarly in the developing hippocampus *in vivo* and in tissue slices cultured *ex vivo.* Anti-GLT-1 immunoreactivity (IR) showed punctate labeling in hippocampal tissues isolated from brains of developing rat (P6 and P12). During the first postnatal week (Fig. 1A–D), at low magnification, GLT-1 IR was most evident as concentrated "patches" or aggregates of GLT-1 puncta above a more dispersed punctate pattern of tissue staining (Fig. 1A,B). Macroscopic patches of GLT-1 IR puncta were similar in size (60–80 μm in diameter) and shape to individual protoplasmic astrocytes in developing hippocampal tissues *in vitro* (Benediktsson et al., 2005) and *in vivo* (Bushong et al., 2004). Indeed, higher magnification images of patches showed more intense GLT-1 puncta appearing over a diffuse, lower level of GLT-1 IR outlining cell bodies and branches (Fig. 1C,D). Double labeling with both GLT-1 and GFAP antibodies confirmed that GLT-1 puncta circumscribed cell bodies and processes of astrocytes (Supp. Info. Fig. 1).

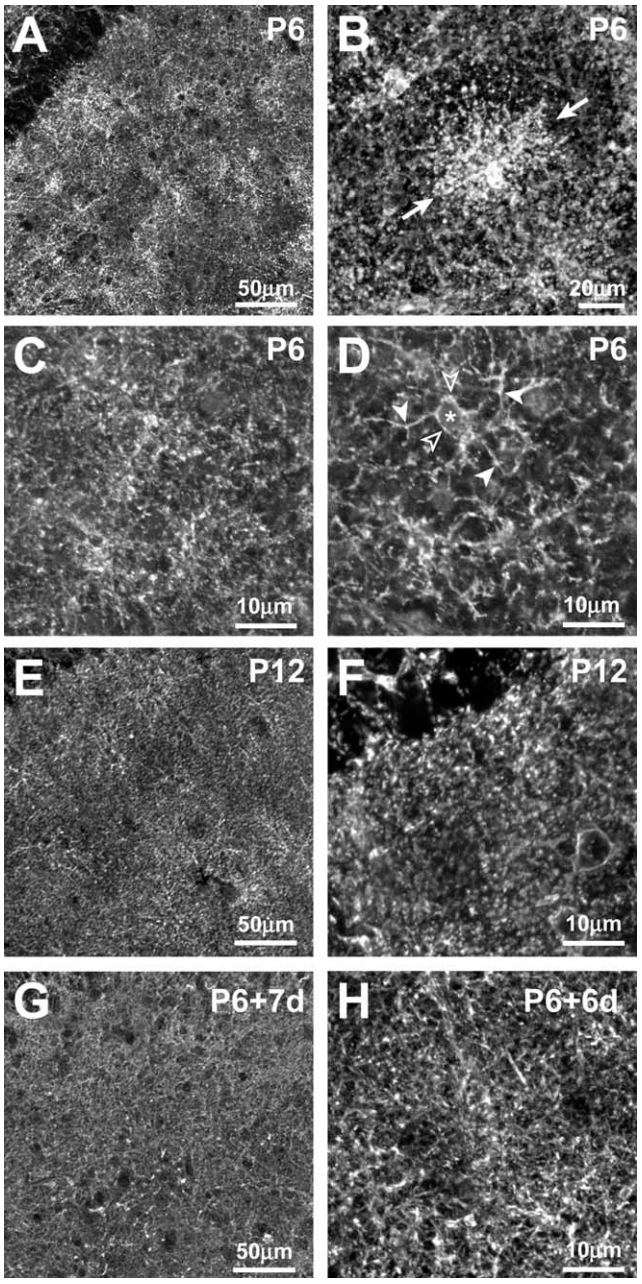

Fig. 1. Anti-GLT-1 antibodies show punctate immunostaining in developing hippocampal area CA1. (**A–D**) GLT-1 immunoreactivity (IR) in hippocampal area CA1 from P6 rat. (A) Low-magnification view of a P6 tissue slice shows nonuniform staining. (B) In some tissues, distinct astrocyte-like "patches" (arrows) are evident above a lower level, more dispersed pattern of punctate staining. A "projection image" of a confocal image stack (C) and a single confocal image plane (D) of the same field of view demonstrate that GLT-1 patches correspond to IR cells whose cell body (* and open arrowheads) and processes (solid arrowheads) are diffusely labeled and bear small, intensely fluorescent puncta (D). (**E** and **F**) Low (E) and high (F) magnification views of a P12 hippocampal slice showing more uniform punctate distribution of GLT-1. Astrocyte-like patches of GLT-1 IR are less prominent at P12. (**G** and **H**) Representative low- (G) and high- (H) magnification views of P6 hippocampal slices cultured for 6–7 days *in vitro* show a GLT-1 distribution similar to that in P12 *in vivo*.

The patchy, astrocyte-like staining pattern was less evident as developmental age increased. In tissues harvested from second postnatal week rat (Fig. 1E,F), the

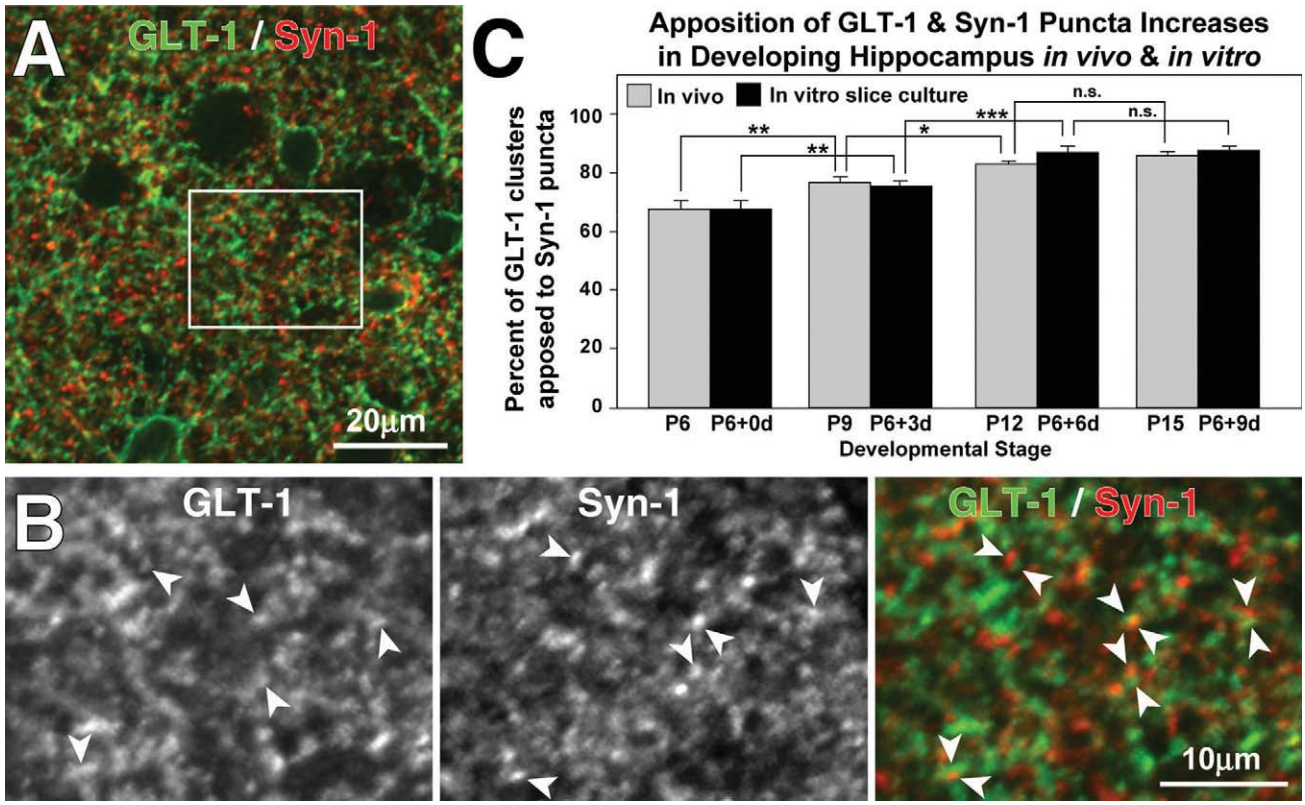

Fig. 2. GLT-1 clusters increasingly localize near synapses as development proceeds. (**A**) Low magnification, single confocal image plane view of P9 hippocampal tissue double labeled for GLT-1 (green) and synapsin-1 (red). (**B**) Boxed region from "A" showing instances of apposition or overlap of syn-1 and GLT-1 (arrowheads). (**C**) Quantitative analyses show that the developmental increase in apposition of GLT-1 and syn-1 immunopuncta is similar in tissues acutely isolated from P6 thru P15 rat and in organotypic slice cultures isolated from P6 rat and cultured for 3, 6, or 9 days *in vitro*. Values shown are mean ± SD and are based on analysis of at least 300 puncta from a minimum of five separate fields of view for each condition. $^{*}P < 0.05$; $^{**}P < 0.02$; $^{***}P < 0.002$. ns = not significant. [Color figure can be viewed in the online issue, which is available at wileyonlinelibrary.com.]

punctate GLT-1 immunostaining was more homogeneous, although occasional cell-like "patches" were seen. A similar GLT-1 staining pattern was observed in tissue harvested from 1-week-old rats and cultured for 1 week, suggesting that this developmental change in GLT-1 distribution also occurs *in vitro* (Fig.1G,H). The patterns and levels of GLT-1 IR were qualitatively similar in acutely isolated (P12) and age-matched cultured tissue slices (P6 + 6 days *in vitro*; cf. Fig. 1E,F and G,H), suggesting that overall expression levels are similar. Previous studies have shown that synaptic density in area CA1 increases during the second postnatal week *in vivo* and in slice cultures (Buchs et al., 1993). Thus, the developmental change in GLT-1 distribution coincides with an increase in the density and complexity of astrocyte processes during maturation (Hama et al., 2004; also Supp. Info. Fig. 1), as well as with the formation and maturation of neuronal synapses.

GLT-1 Clusters are Increasingly Localized near Synapses as Development Proceeds

GLT-1 has been shown to limit the activation of NMDA and metabotropic GluRs (Huang et al., 2004; Tanaka et al., 1997) and to alter the threshold for induction of long-term potentiation (LTP) in area CA1 (Katagiri et al., 2001), suggesting that it is localized near excitatory synapses. To determine if GLT-1-positive (GLT-1+) puncta were localized near synaptic structures, we coimmunostained acutely isolated hippocampal slices for GLT-1 and a presynaptic terminal protein, Synapsin-1 (syn-1; Fig. 2A,B). Three-dimensional analysis of confocal image stacks showed that at P6, 68% of GLT-1+ clusters (n = 314) in area CA1 were within 1 μm of a synapsin-1-positive (syn-1+) punctum, and by P15 the degree of apposition increased to 86% (n = 415 GLT-1 clusters) (Fig. 2C). This developmental increase in synaptic apposition of GLT-1 *in vivo* was recapitulated in organotypic slice cultures *in vitro* (Fig. 2C). Together, these results suggest that GLT-1 in astrocytes is organized into discrete clusters that are preferentially localized to sites near neural synapses.

GFP-GLT-1 Forms Discrete Clusters in Hippocampal Astrocytes *In Situ*

Excitatory synapses form rapidly between hippocampal neurons when growing axons encounter motile dendritic filopodia (Friedman et al., 2000). The expression of GLT-1 by astrocytes precedes the formation of excitatory synapses (Shibata et al., 1996), raising the possibility

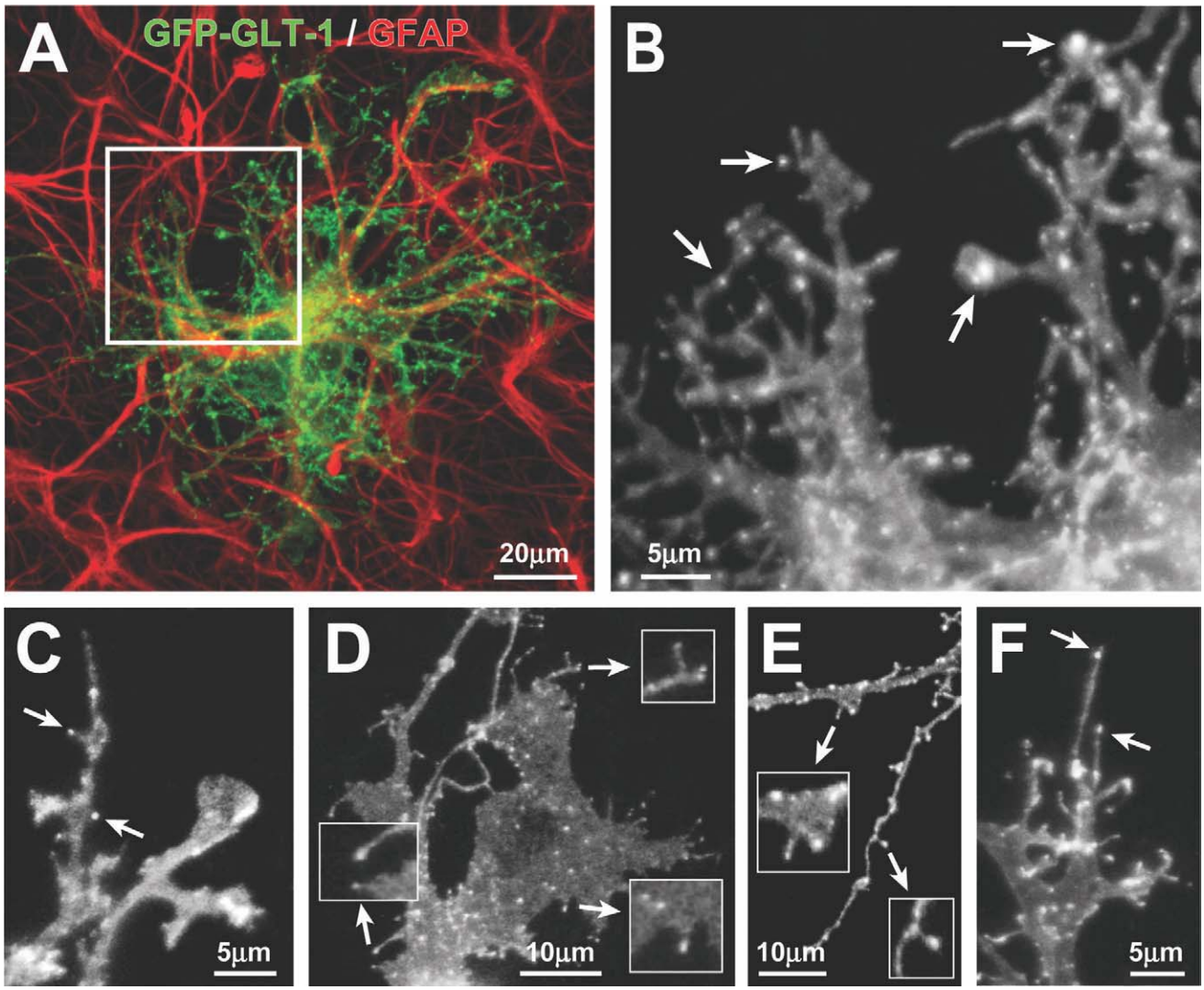

Fig. 3. GFP-GLT-1 in transfected astrocytes in slice cultures is concentrated in clusters within lamellae, spine-like, and filopodia-like processes. (**A**) Low-magnification view of a CA1 hippocampal astrocyte in a P6 + 5 days *in vitro* (DIV) slice culture expressing GFP-GLT-1 (green) and immunostained for GFAP (red). (**B**) Higher magnification view showing intensely fluorescent GFP-GLT-1 clusters (arrows) against a lower level of diffuse fluorescence in astrocytic processes. (**C–F**) Examples of GFP-GLT-1 clusters in short, spine-like structures (C–E, arrows) and at the tips of longer filopodia-like structures (F, arrows). Numerous GFP-GLT-1 clusters are distributed over the surface of sheet-like lamellipodia (D) and line the edges of astrocyte processes (E). [Color figure can be viewed in the online issue, which is available at wileyonlinelibrary.com.]

that preformed GLT-1 clusters could move to regions where astrocyte lamellipodia contact nascent synapses. To determine the subcellular distribution of GLT-1 in individual astrocytes and to monitor the movement of GLT-1 clusters over time, we used ballistics to randomly transfect a few astrocytes in developing organotypic slices with cDNA encoding a GFP-GLT-1 fusion protein. We restricted our analysis to astrocytes (n = 36) within the stratum radiatum of area CA1 because hippocampal slice cultures retain the intrinsic Schaffer collateral projection to area CA1 (Gahwiler et al., 1997), and this region represents a well characterized model for studying astrocyte-synapse relationships (Ventura and Harris, 1999). As expected for proteins targeted to the plasma membrane of astrocytes *in situ* (Benediktsson et al., 2005), expression of GFP-GLT-1 revealed the fine lamellipodia and filopodia of these complex cells (Fig. 3A). In higher magnification views of transfected astrocytes, individual GFP-GLT-1 clusters or "hotspots" of transporter accumulation were visible over a lower level, diffuse membrane fluorescence (Fig. 3B). GFP-GLT-1 clusters, defined as discrete spots of fluorescence intensity at least two times greater than the diffuse membrane fluorescence, had an average diameter of 1.1 ± 0.04 μm (n = 100). This was nearly identical to the diameter of GLT-1+ immunolabeled puncta (1.1 ± 0.16 μm; n = 40 clusters from four cells), indicating that expression of GFP-GLT-1 does not greatly inflate cluster size. GFP-GLT-1 clusters were observed on the cell body and along processes. GFP-GLT-1 clusters were also seen on the surfaces and edges of lamellipodia, and at the tips of filopodia and bulbous spine-like structures (Fig. 3C–F),

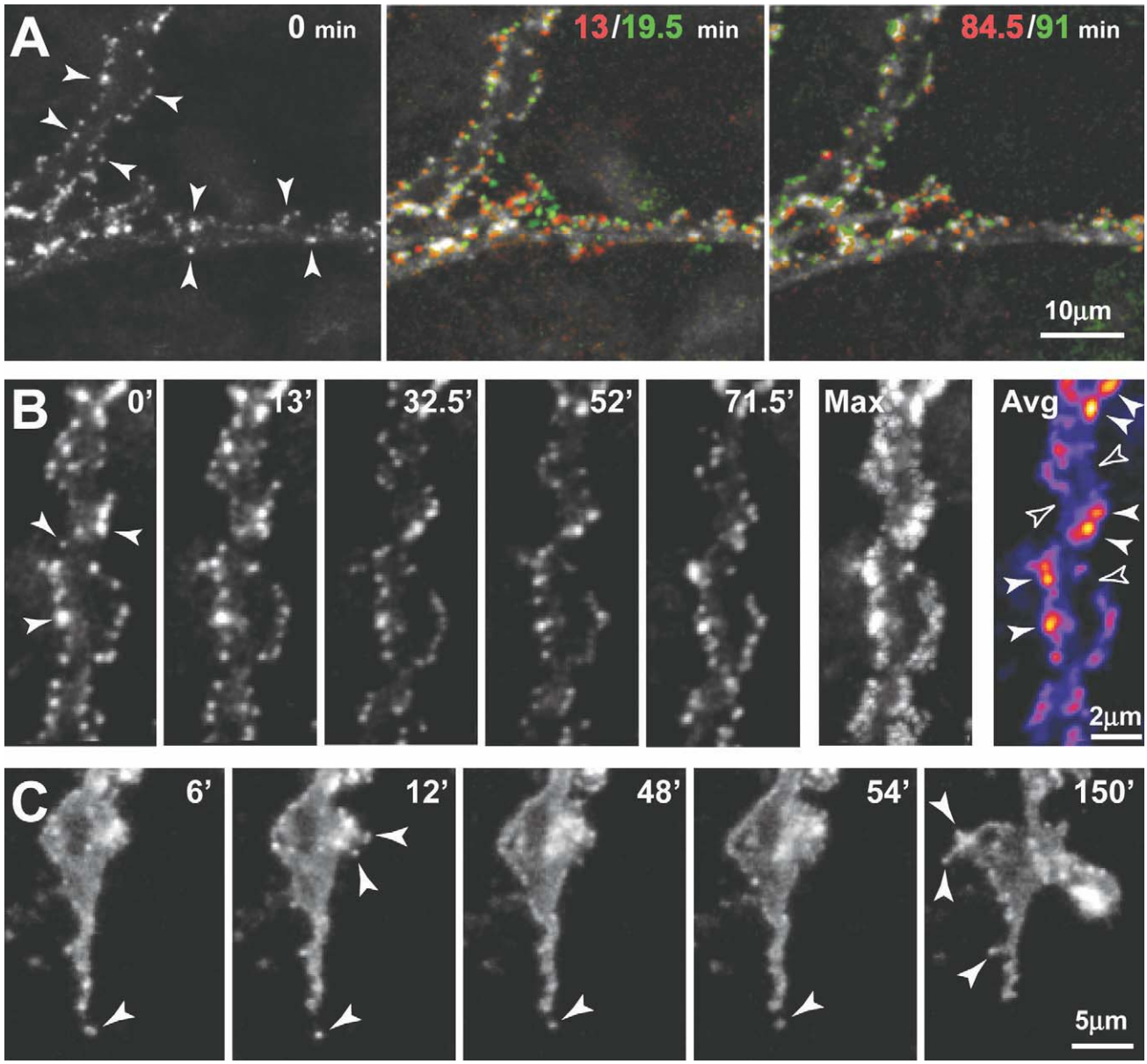

Fig. 4. Time-lapse imaging shows remodeling of GFP-GLT-1 clusters in developing astrocytes *in situ*. (**A**) Left image shows portions of two processes near the margin of a GFP-GLT-1-expressing astrocyte (P6 + 6 DIV slice culture). Note the GFP-GLT-1 clusters (arrowheads) positioned along the edges of the processes. Color composite images (center and right) show changes in cluster position in pairs of time-points (encoded red and green, respectively), 6.5 min apart, near the beginning (13/19.5 min) and end (84.5/91 min) of a ~ 90 min imaging session. Clusters that do not change position between time-points appear white. Note that many GFP-GLT-1 clusters move within the 6-min intervals, although some are stable. Image in panels A and B are *z*-stack projections of nine focal planes. (**B**) Representative images from a time-lapse sequence shows remodeling of GFP-GLT-1 clusters in the top astrocyte process in panel A. Note that clusters of differing sizes line the edges of the processes (arrowheads at 0 min). Although most clusters change position slightly from frame to frame, many individual clusters can be followed over the ~ 90 min sequence. The "Max" image is a maximum brightness composite showing the peak intensities across all 16 time points in the sequence, thereby representing the area sampled by the clusters in this astrocyte branch over a 90-min period of time. The "Avg" image shows average intensity at each position over the time sequence, with a pseudo-color look-up table applied to indicate regions showing greater average GLT-1 cluster occupancy. These "cumulative time" images show areas of high (solid arrowheads) and low cluster occupancy (open arrowheads) along single astrocyte branches. See Supporting Information Video. (**C**) Remodeling of GFP-GLT-1 clusters at the growing tip of a developing astrocyte branch that undergoes cycles of extension and retraction. Short, spine-like structures on growing astrocyte branches extend and retract, carrying along GFP-GLT-1 clusters. A GFP-GLT-1 cluster retracts along with a thin filopodium at the tip of the branch (bottom arrowhead, 6–54 min). Meanwhile, some small spine-like structures containing GFP-GLT-1 clusters extend from another region of the astrocyte process (upper arrowheads, 12 min). Later, three spine-like structures extend (arrowheads, 150 min) and persist for the remainder of the time-lapse sequence (total time = 4.45 h). See Supporting Information Video. [Color figure can be viewed in the online issue, which is available at wileyonlinelibrary.com.]

while some fine astrocyte processes lacked GFP-GLT-1+ clusters. Analysis of individual astrocytes coexpressing GFP-GLT-1 and DsRed2, a cytosolic fluorescent protein, confirmed that GFP-GLT-1 is targeted to the plasma membrane and that GFP-GLT-1 clusters represent sites of protein concentration (Supp. Info. Figs. 2 and 3).

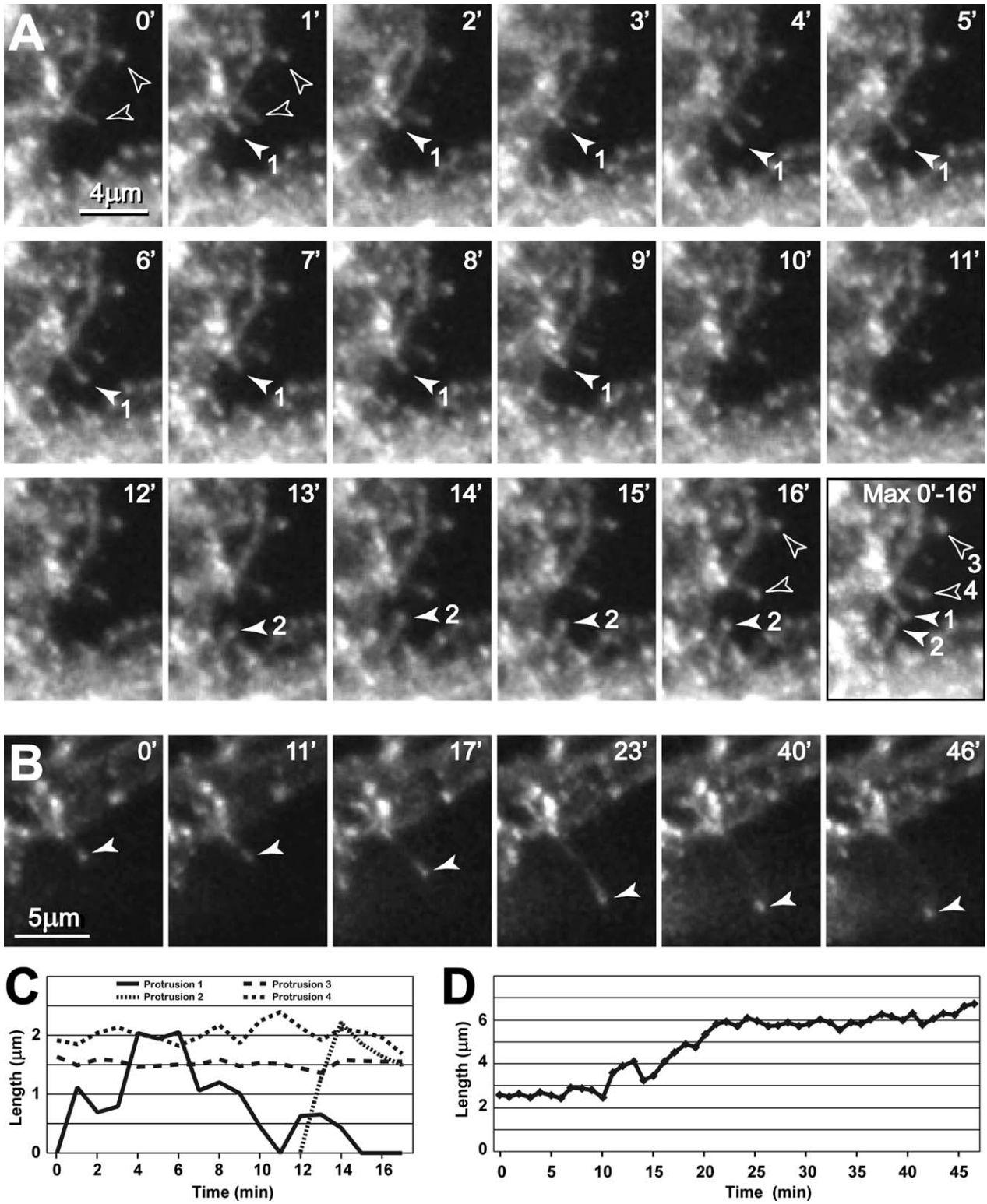

Fig. 5. Remodeling of GLT-1 clusters associated with lateral filopodia on developing astrocytes. (**A**) High-magnification, time-lapse sequence of a region at the margin of a GFP-GLT-1 expressing astrocyte shows remodeling of four filopodia and spine-like protrusions (numbered 1–4 in the "Max" projection image) over a 16-min period of time (confocal stacks of images taken every 1 min). Some protrusions transiently extend and retract (solid arrowheads; 1, 2), while others persist and do not change (open arrowheads; 3, 4). Each protrusion reaches a peak length of $\sim$ 2 μm. The last panel is a maximum brightness composite of all time-points showing the area sampled by the protrusions during a 16 min period. See Supporting Information Video. (**B**) Different region of the same cell shows a persistent protrusion that elongates from $\sim$ 2 μm to over 6 μm long within a 15-min period of time, carrying along a GFP-GLT-1 cluster at its tip as it grows. See Supporting Information Video. (**C, D**) Graphs of protrusion length for the structures shown in panels A and B, respectively.

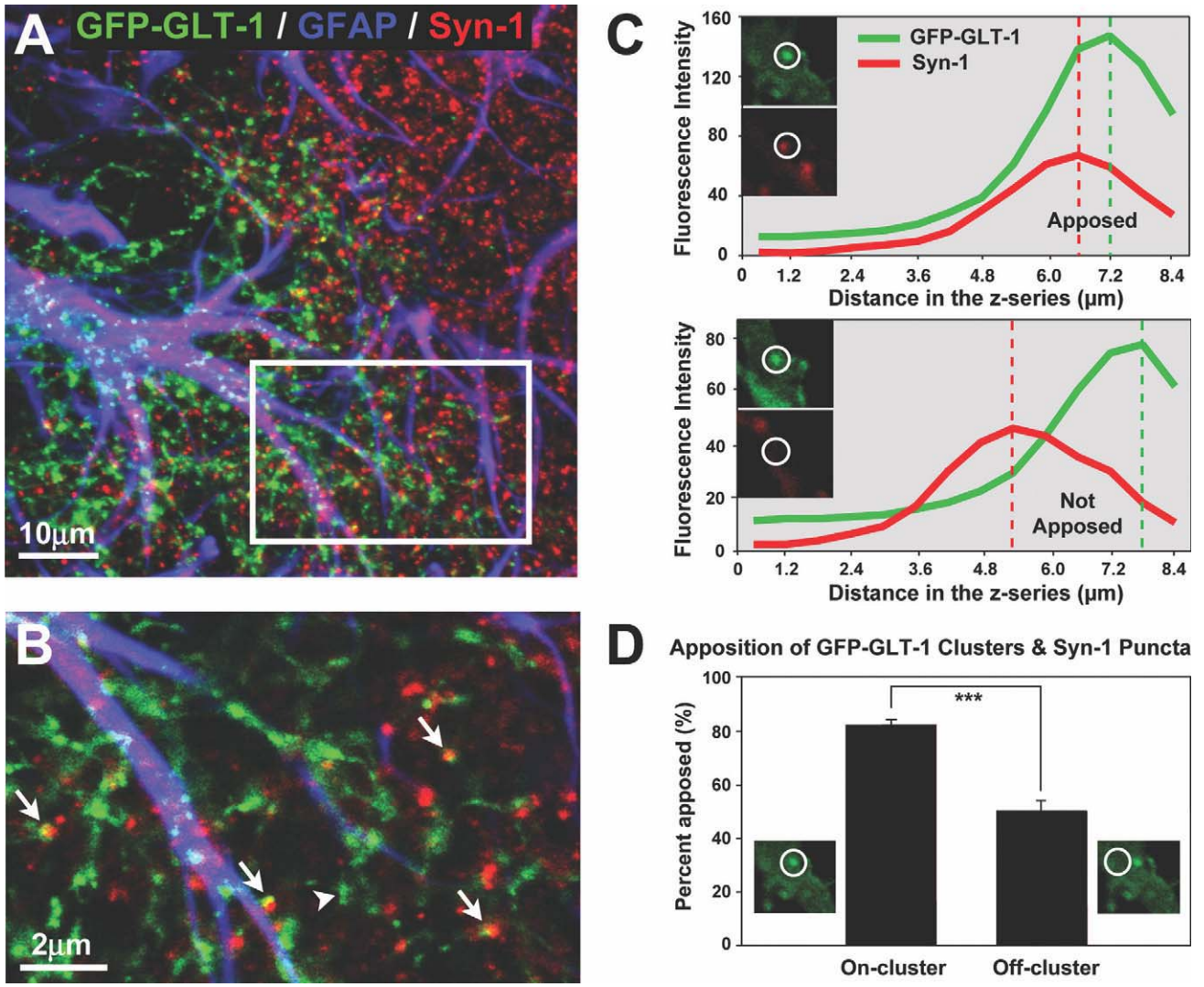

Fig. 6. GFP-GLT-1 clusters often adjoin synapsin-1-positive presynaptic terminals. (**A**) Low-magnification, three-channel merged image of a region of an astrocyte transfected with GFP-GLT-1 (green) and, after 48 hr, fixed and immunostained for GFAP (blue) and synapsin-1 (syn-1, red). The image represents a projection of 10 *z*-plane optical sections spanning ~ 8μm. (**B**) Single confocal image plane from boxed region in (A) showing close apposition or overlap (yellow) of GFP-GLT-1 clusters and anti-syn-1 immunopuncta (arrows). Some GFP-GLT-1 clusters do not adjoin synapsin-I puncta (arrowhead). (**C**) Analysis of apposition of GFP-GLT-1 clusters and syn-1 puncta. Upper panel: A 2-μm diameter region-of-interest (ROI) is centered on a GFP-GLT-1 cluster and an adjoining syn-1 immunopunctum in a single confocal image plane. The plot of mean fluorescence intensity along the *z*-axis for the ROI shows that the green and red channel intensity peaks are within 1 μm of each other, thereby meeting our criteria for apposition. Lower panel: A 2-μm diameter ROI is centered on a GFP-GLT-1 cluster that does not adjoin a syn-1 immunopunctum. In this instance, the peak fluorescence intensity of a syn-1 punctum in the red channel is not within 1 μm of the peak intensity of the green channel, and thus is not considered apposed. (**D**) Sites on transfected astrocytes that contain GFP-GLT-1 clusters are much more frequently localized near syn-1 immunopuncta than sites that do not contain GLT-1 clusters (off-cluster, randomized control). These data indicate a preferential localization of GFP-GLT-1 clusters near synaptic structures. ***$P < 0.001$. [Color figure can be viewed in the online issue, which is available at wileyonlinelibrary.com.]

Time-Lapse Imaging Reveals Dynamic Remodeling of GFP-GLT-1 Clusters in Developing Astrocytes

To assess whether GFP-GLT-1 clusters represent stable accumulations of transporters or dynamic structures that can be remodeled over time, we examined GFP-GLT-1 clusters in astrocytes in live tissue slices using time-lapse confocal microscopy. To monitor dynamic changes in three dimensions and circumvent problems associated with focal drift, we collected stacks of confocal optical sections every 4–6 min for up to 10 h. Analysis of time-lapse movies ($n = 7$ cells) revealed that GFP-GLT-1 clusters in developing astrocytes display a variety of dynamic behaviors (Fig. 4A). Many clusters along the shafts of astrocytic processes were mobile, moving along the edges of processes (Fig. 4B and Supp. Info. Video). Moving clusters sometimes appeared to merge or disappear from view. “Cumulative time" images showed a nonuniform distribution of GLT-1 clusters over time; some regions of astrocyte branches had “hotspots" with many GFP-GLT-1 clusters, whereas other regions showed a paucity of clusters (Fig. 4B Avg). At the growing tips of astrocytes, GFP-GLT-1 clusters were carried along with branches and filopodia as they extended and

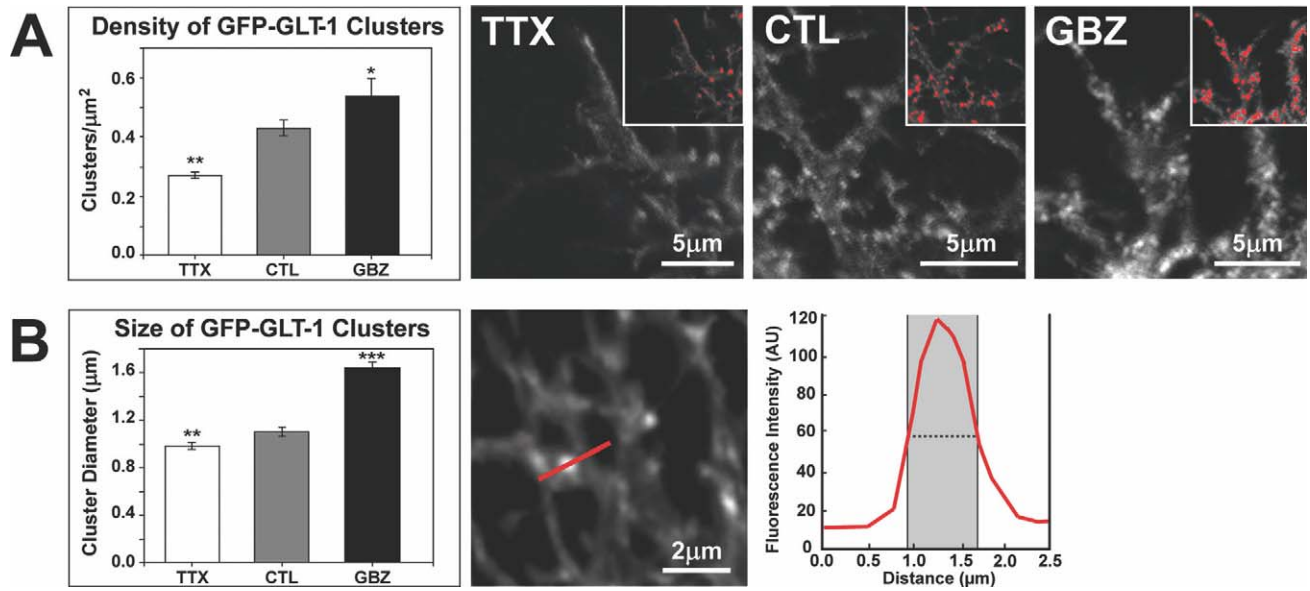

Fig. 7. Synaptic transmission regulates the size and density of GFP-GLT-1 clusters. (**A**) As synaptic transmission increases, there is a corresponding increase in the density of GFP-GLT-1 clusters, from 0.27 clusters/μm^2 in the activity blockade (TTX) condition, to 0.43 clusters/μm^2 in control (CTL) condition, and 0.54 clusters/μm^2 in GBZ treated slices. Portions of transfected astrocytes under TTX, CTL, or GBZ conditions are shown at right. Insets show suprathreshold regions (red) that were considered clusters for the quantitative analysis (see Methods for details). (**B**) The mean diameter of individual GFP-GLT-1 clusters increases as synaptic activity increases. Cluster diameter was defined as the full width at half maximum fluorescent intensity (shaded region in graph) along a line bisecting the cluster. Student's *t*-test. $^*P < 0.05$, $^{**}P < 0.01$, $^{***}P < 0.001$. [Color figure can be viewed in the online issue, which is available at wileyonlinelibrary.com.]

retracted (Fig. 4C). Although many clusters moved short distances over a period of minutes, only rarely did clusters translocate long distances along the shafts of astrocyte processes, suggesting that most clusters are integral plasma membrane components rather than intracellular transport vesicles.

When images were captured at short (1 min) time intervals, GFP-GLT-1 clusters were observed to move along with filopodia-like structures that projected laterally from astrocyte branches as they extended and retracted (Fig. 5A). Some filopodia- or spine-like structures bearing clusters at their tips were relatively stable, showing no appreciable change in length for at least several minutes (Fig. 5A,C). Although most filopodia were rather short ($\sim$ 2 μm), some filopodia carrying a GFP-GLT-1 cluster were over 6 μm in length (Fig. 5B,D). Such long filopodia have been observed previously on astrocytes *in vivo* at this developmental stage (Bushong et al., 2004), indicating that they are not abnormal structures induced by GFP-GLT-1 expression. These observations indicate that clusters of GLT-1 can move along the surface of developing astrocyte processes, and emerge with growing lamellipodial and filopodial structures.

Most GFP-GLT-1 Clusters are Situated Adjacent to Presynaptic Terminals

To determine the relationship of GFP-GLT-1 clusters to synapses, slice cultures containing transfected astrocytes were immunostained with anti-syn-1 antibodies. In single confocal image planes through transfected astrocytes, many but not all GFP-GLT-1 clusters were located adjacent to, or overlapping with, syn-1+ puncta (Fig. 6A,B). To further investigate this association in three-dimensions, we assessed the apposition of GFP-GLT-1 clusters and syn-1+ puncta in through-focus stacks of confocal images from 6- to 7-day-old slice cultures. We found that 82% of GLT-1 clusters (n = 332 clusters from 20 cells) were located within 1 μm of a syn-1+ punctum, whereas only 50% of randomly selected regions of an astrocyte that lacked discrete GFP-GLT-1 clusters were closely adjoining syn-1+ puncta ($P < 0.0001$; Fig. 6C,D). These results indicate that clusters of GFP-GLT-1 are preferentially located near synapses.

Neuronal Activity Influences GFP-GLT-1 Cluster Size and Density

Chronic alterations in neuronal activity are associated with changes in GluT expression (Wong et al., 2003), and transection of afferent inputs reduces GLT-1 expression in the target field (Ginsberg et al., 1995), suggesting that GluT expression can be regulated by neuronal activity. To determine if changes in neuronal activity alter GLT-1 clusters in astrocytes, we cultured organotypic slices for 7 days in either 0.2 μM TTX, no drug (control, CTL), or for 24-h post-transfection in 10 μM GBZ. Examination of treated slices revealed that GFP-GLT-1 cluster density was decreased by 37% from control when action potential firing was blocked by TTX (n = 25 image planes from six cells, $P < 0.01$), whereas cluster density was increased by 25% when neuronal activity was

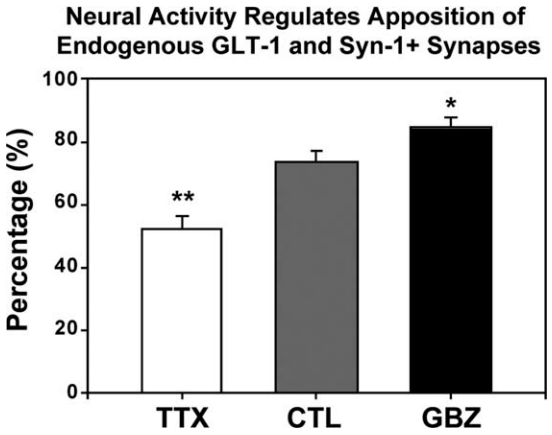

Fig. 8. Synaptic transmission regulates synaptic apposition of endogenous GLT-1. Graph shows percentage of GLT-1 immunopuncta apposed to syn-1 immunopuncta in TTX, control, and GBZ conditions in slice cultures. TTX significantly decreased apposition of GLT-1 immunopuncta ($n = 262$) with synapses, whereas GBZ treatment significantly increased the apposition of GLT-1 puncta ($n = 174$) with synapses. Student's t-test. $^*P < 0.05$, $^{**}P < 0.01$.

enhanced by GBZ ($n = 36$ image planes from nine cells, $P < 0.05$; Fig. 7A). Furthermore, the mean size of GFP-GLT-1 clusters increased by 49%, from 1.1 ± 0.04 μm ($n = 100$ clusters) to 1.6 ± 0.06 μm ($n = 80$ clusters) when neuronal activity was enhanced by GBZ ($P < 0.0001$; Fig. 7B). There was also a small but significant ($P < 0.01$) decrease in cluster size when neural activity was blocked (TTX). These findings indicate that global changes in neuronal activity alter both the size and density of cell surface GluT clusters in developing astrocytes.

Synaptic Transmission Recruits Endogenous GLT-1 to Synaptic Sites

Chronic changes in neuronal activity can induce presynaptic and postsynaptic homeostatic plasticity, including changes in the probability of glutamate release from nerve terminals and in the density of synapses (Turrigiano, 2007). If proper localization of GLT-1 is important for clearance of glutamate at excitatory synapses, the dynamic movement and apposition of GLT-1 clusters to synapses should also be influenced by changes in neuronal activity. Consistent with this hypothesis, there was a 53% decrease in apposition of endogenous GLT-1 clusters with syn-1+ puncta ($P < 0.01$) in slices cultured in TTX ($n = 262$ GLT-1 clusters, eight cells) (Fig. 8). Conversely, there was a 15% increase ($P < 0.05$) in apposition between GLT-1 clusters and syn-1 puncta ($n = 174$ clusters, six cells) in slices exposed to GBZ (Fig. 8). Together, these data indicate that neural activity bidirectionally regulates the perisynaptic localization of GLT-1 clusters.

DISCUSSION

Here we demonstrate that GLT-1, the predominant GluT expressed in brain, assembles into discrete clusters in astrocyte membranes that are positioned near synapses. Pharmacologically induced alterations in neuronal activity in developing brain tissues resulted in concomitant changes in the size and abundance of these transporter clusters near sites of release, suggesting that GluT availability is regulated by the frequency of transmitter release at excitatory synapses. The existence of dynamic clusters of GLT-1 that are responsive to changes in neuronal activity provides further evidence that astrocytes respond to and modulate transmission at the level of single synapses.

Perisynaptic Localization of GLT-1 Clusters

Previous EM-level analyses of rat hippocampus indicate that many spine synapses are contacted by astrocyte processes *in vivo* (76%, Ventura and Harris, 1999; Witcher et al., 2007) and in cultured tissue slices *in vitro* (85%; Lushnikova et al., 2009). Our data showing that ~ 82% of GLT-1 clusters are located within 1 μm of a synapse are consistent with these findings, and suggest that many synaptically associated astrocytic processes *in situ* contain GLT-1 clusters. GLT-1 also may regulate glutamate levels near GABAergic synapses to alter heterosynaptic interactions. However, a previous confocal study in rat neocortex found that a larger fraction of GLT-1 is intimately associated with excitatory terminals than with inhibitory terminals immunolabeled for the gamma-aminobutyric acid (GABA) transporter, VGAT (Minelli et al., 2001).

Neural Activity Regulates GLT-1 Clustering

Modification of individual synapses is thought to underlie key aspects of learning and memory, and is manifested through changes in synaptic features such as the type and number of receptors (Newpher and Ehlers, 2008), the size and shape of dendritic spines (Alvarez and Sabatini, 2007), and possibly the number of synaptic contacts (Desmond and Levy, 1986; Stewart et al., 2000). The prominent role of GLT-1 in buffering and clearing synaptic glutamate suggests that it may be coregulated in response to changes in synaptic activity. In accordance with this hypothesis, astrocytes *in vitro* increase expression of GLT-1 when cocultured with neurons (Swanson et al., 1997; Perego et al., 2000) or when exposed to neuron-conditioned media (Gegelashvili et al., 1997). Furthermore, enhancement of neuronal activity *in vivo* through repetitive sensory stimulation induces robust increases in GLT-1 expression in corresponding cortical regions (Genoud et al., 2006), and chronic restraint stress enhances GLT-1 expression in regions that exhibit extensive dendritic remodeling (Reagan et al., 2004). Conversely, transection of afferent fibers decreases GLT-1 levels in target zones (Ginsberg et al., 1995; Hein et al., 2001; Lievens et al., 2000), and GLT-1 expression is altered in a variety of neurological diseases, such as amyotrophic lateral sclerosis (Howland et al., 2002; Lin et al., 1998; Vanoni et al., 2004), schizo-

phrenia (Matute et al., 2005), and following acute ischemic brain injury (Rao et al., 2001), indicating that GLT-1 expression is tightly regulated. Our results indicate that alterations in neuronal activity not only induce changes in GLT-1 expression but also alter the spatial organization of GluTs in astrocyte membranes, pointing to an important role for synaptic activity in regulating the formation, growth, and spatial arrangement of GLT-1 clusters, including the recruitment of GLT-1 clusters to perisynaptic locations.

GLT-1 and Synaptic Homeostasis

Changes in the expression level or position of GluTs in astrocytes may reflect homeostatic responses to neural activity. Homeosynaptic plasticity is a phenomenon whereby a global change in activity results in a "scaling" of synapse strength so that the relative strength of individual synapses can be maintained when there is a global change in activity (Davis, 2006; Turrigiano, 2007). In this model, chronic activity deprivation induces an increase in the number of synaptic GluRs while enhanced activity causes a decrease in receptor number (Lissin et al., 1998; O'Brien et al., 1998; Turrigiano et al., 1998), an effect that can manifest at the level of individual synapses (Hou et al., 2008). We found that chronic exposure of hippocampal slices to TTX significantly reduced the size and density of GLT-1 clusters and decreased the number of these clusters that were adjacent to synapses; conversely, enhancing activity by exposure to GBZ resulted in an increase in the number of GLT-1 clusters and closer apposition of these clusters to synapses. Astrocytes, therefore, also exhibit homeostatic changes in response to global changes in neuronal activity, scaling back the number and density of GluTs near release sites when demand is reduced. These results suggest that the most active synapses may recruit additional GluTs to provide additional capacity for buffering or clearance, perhaps to ensure that receptors in synaptic and perisynaptic domains are not subjected to prolonged glutamate transients or spillover from adjacent, highly active synapses.

GLT-1 Cluster Dynamics

Our data indicate several possible modes of GLT-1 recruitment to perisynaptic sites: clusters may translocate to perisynaptic sites within stable astrocytic processes; astrocytic processes may extend toward synapses, carrying along GLT-1 clusters; or clusters may form *de novo* at perisynaptic sites within ensheathing astrocytic processes. The relative contributions of these different modes of delivery are presently unknown and may differ depending on developmental and physiological contexts. Additional studies will be required to determine whether neural activity regulates the rates of formation, movement, or turnover of GLT-1 clusters.

In principle, localization of GLT-1 in astrocytes may involve mechanisms similar to trafficking of GluRs in neurons, in which receptors insert into the plasma membrane and shuttle between synaptic and extrasynaptic locations by lateral diffusion (see Renner et al., 2008). GluRs exhibit a range of mobility behaviors, and localization depends on interactions with cytoskeletal-associated scaffolding proteins that restrict diffusion (Newpher and Ehlers, 2008). Likewise, GLT-1 localization in astrocytes may involve the actin cytoskeleton (Zhou and Sutherland, 2004), possibly through interactions with a LIM protein, Ajuba (Marie et al., 2002).

The rates of GLT-1 clustering and remodeling are likely to have functional consequences for synaptic development and plasticity. Depending on the timing and rate of GLT-1 recruitment, nascent synapses lacking astrocytic ensheathment may have greater potential for activating extrasynaptic mGluRs and NMDA receptors, if localization of glial transporters lags behind the formation of neuronal synaptic machinery. Two previous time-lapse studies (Haber et al., 2006; Nishida and Okabe, 2007) investigating the relationship of astrocytic remodeling to neuronal spine dynamics support the notion that astrocytes can modulate the development of synaptic structures by directly contacting dendritic spine precursors (filopodia). This interaction may help stabilize newborn synapses and promote spine maturation. Our time-lapse data complement these studies by identifying mobile, preformed GluT clusters within developing astrocyte branches *in situ*, thereby suggesting that GluTs can be rapidly delivered to or retrieved from newly formed synapses in response to local synaptic activity.

Although the mechanisms by which synaptic transmission regulates astrocyte development and synaptic ensheathment remain to be fully elucidated, a previous study has shown that local application of glutamate induces growth of filopodia-like structures on cultured astrocytes *in vitro* (Cornell-Bell et al., 1990), suggesting that glutamate spillover from active synapses may induce astrocyte process outgrowth (Witcher et al., 2007). Indeed, imaging studies in tissue slices indicate that astrocytic processes near active synapses are motile, extending sheet-like and filopodia-like protrusions (Benediktsson et al., 2005; Hirrlinger et al., 2004). EM studies in slice cultures have shown that synaptic potentiation induces increased glial coverage of excitatory synapses in hippocampal area CA1 (Lushnikova et al., 2009), consistent with the hypothesis that astrocytic processes preferentially surround synapses that have more glutamate escaping from their perimeters (Ventura and Harris, 1999). Such activity-dependent remodeling of astrocyte structure and neuron-astrocyte interactions (Theodosis et al., 2008) may explain the variability in astrocyte ensheathment of excitatory synapses in the hippocampus (Ventura and Harris, 1999).

Together, our results suggest that mobile GluT clusters may contribute to rapid spatial and temporal regulation of glutamatergic signaling at the level of individual synapses. Activity-dependent recruitment and

regulation of GluTs within dynamic perisynaptic glial processes supports the hypothesis that neuronal and glial components of the tripartite synapse work together to ensure optimal signaling. Greater insight into the molecular mechanisms that regulate GluT localization and remodeling may help elucidate how abnormal signaling between neuronal and glial elements contributes to developmental abnormalities and altered CNS function in disease.

REFERENCES

Alvarez VA, Sabatini BL. 2007. Anatomical and physiological plasticity of dendritic spines. Annu Rev Neurosci 30:79–97.

Benediktsson AM, Schachtele SJ, Green SH, Dailey ME. 2005. Ballistic labeling and dynamic imaging of astrocytes in organotypic hippocampal slice cultures. J Neurosci Methods 141:41–53.

Bergles DE, Jahr CE. 1997. Synaptic activation of glutamate transporters in hippocampal astrocytes. Neuron 19:1297–1308.

Buchs P-A, Stoppini L, Muller D. 1993. Structural modifications associated with synaptic development in area CA1 of rat hippocampal organotypic cultures. Dev Brain Res 71:81–91.

Bushong EA, Martone ME, Ellisman MH. 2004. Maturation of astrocyte morphology and the establishment of astrocyte domains during postnatal hippocampal development. Int J Dev Neurosci 22:73–86.

Butchbach ME, Tian G, Guo H, Lin CL. 2004. Association of excitatory amino acid transporters, especially EAAT2, with cholesterol-rich lipid raft microdomains: Importance for excitatory amino acid transporter localization and function. J Biol Chem 279:34388–34396.

Chaudhry FA, Lehre KP, van Lookeren Campagne M, Ottersen OP, Danbolt NC, Storm-Mathisen J. 1995. Glutamate transporters in glial plasma membranes: Highly differentiated localizations revealed by quantitative ultrastructural immunocytochemistry. Neuron 15:711–720.

Cornell-Bell AH, Thomas PG, Smith SJ. 1990. The excitatory neurotransmitter glutamate causes filopodia formation in cultured hippocampal astrocytes. Glia 3:322–334.

Dailey ME, Manders E, Soll DR, Terasaki M. 2006. Confocal microscopy of living cells. In: Pawley JB, editor. Handbook of biological confocal microscopy, 3rd ed. New York: Springer. pp 381–403.

Dailey ME, Marrs GS, Kurpius D. 2011. Maintaining live cells and tissue slices in the imaging setup. In: Helmchen F, Konnerth A, Yuste R, editors. Imaging in neuroscience: A laboratory manual. Cold Spring Harbor Laboratory Press: Cold Spring Harbor, NY. pp 331–338.

Danbolt NC. 2001. Glutamate uptake. Prog Neurobiol 65:1–105.

Dani JW, Chernjavsky A, Smith SJ. 1992. Neuronal activity triggers calcium waves in hippocampal astrocyte networks. Neuron 8:429–440.

Davis GW. 2006. Homeostatic control of neural activity: From phenomenology to molecular design. Annu Rev Neurosci 29:307–323.

Davis KE, Straff DJ, Weinstein EA, Bannerman PG, Correale DM, Rothstein JD, Robinson MB. 1998. Multiple signaling pathways regulate cell surface expression and activity of the excitatory amino acid carrier 1 subtype of Glu transporter in C6 glioma. J Neurosci 18:2475–2485.

Derouiche A, Heimrich B, Frotscher M. 1993. Loss of layer-specific astrocytic glutamine synthetase immunoreactivity in slice cultures of hippocampus. Eur J Neurosci 5:122–127.

Desmond NL, Levy WB. 1986. Changes in the numerical density of synaptic contacts with long-term potentiation in the hippocampal dentate gyrus. J Comp Neurol 253:466–475.

Friedman HV, Bresler T, Garner CC, Ziv NE. 2000. Assembly of new individual excitatory synapses: Time course and temporal order of synaptic molecule recruitment. Neuron 27:57–69.

Furuta A, Rothstein JD, Martin LJ. 1997. Glutamate transporter protein subtypes are expressed differentially during rat CNS development. J Neurosci 17:8363–8375.

Gähwiler BH, Capogna M, Debanne D, McKinney RA, Thompson SM. 1997. Organotypic slice cultures: A technique has come of age. Trends Neurosci 20:471–477.

Gegelashvili G, Danbolt NC, Schousboe A. 1997. Neuronal soluble factors differentially regulate the expression of the GLT1 and GLAST glutamate transporters in cultured astroglia. J Neurochem 69:2612–2615.

Genoud C, Quairiaux C, Steiner P, Hirling H, Welker E, Knott GW. 2006. Plasticity of astrocytic coverage and glutamate transporter expression in adult mouse cortex. PLoS Biol 4:e343.

Ginsberg SD, Martin LJ, Rothstein JD. 1995. Regional deafferentation down-regulates subtypes of glutamate transporter proteins. J Neurochem 65:2800–2803.

Ginsberg SD, Rothstein JD, Price DL, Martin LJ. 1996. Fimbria-fornix transections selectively down-regulate subtypes of glutamate transporter and glutamate receptor proteins in septum and hippocampus. J Neurochem 67:1208–1216.

Haas KZ, Sperber EF, Opanashuk LA, Stanton PK, Moshé SL. 2001. Resistance of immature hippocampus to morphologic and physiologic alterations following status epilepticus or kindling. Hippocampus 11:615–625.

Haber M, Zhou L, Murai KK. 2006. Cooperative astrocyte and dendritic spine dynamics at hippocampal excitatory synapses. J Neurosci 26:8881–8891.

Hama K, Arii T, Katayama E, Marton M, Ellisman MH. 2004. Tridimensional morphometric analysis of astrocytic processes with high voltage electron microscopy of thick Golgi preparations. J Neurocytol 33:277–285.

Hein C, Horváth E, Kugler P. 2001. Glutamate transporter expression in astrocytes of the rat dentate gyrus following lesion of the entorhinal cortex. Eur J Neurosci 13:1839–1848.

Hirrlinger J, Hülsmann S, Kirchhoff F. 2004. Astroglial processes show spontaneous motility at active synaptic terminals *in situ*. Eur J Neurosci 20:2235–2239.

Hou Q, Zhang D, Jarzylo L, Huganir RL, Man HY. 2008. Homeostatic regulation of AMPA receptor expression at single hippocampal synapses. Proc Natl Acad Sci USA 105:775–780.

Howland DS, Liu J, She Y, Goad B, Maragakis NJ, Kim B, Erickson J, Kulik J, DeVito L, Psaltis G, DeGennaro LJ, Cleveland DW, Rothstein JD. 2002. Focal loss of the glutamate transporter EAAT2 in a transgenic rat model of SOD1 mutant-mediated amyotrophic lateral sclerosis (ALS). Proc Natl Acad Sci USA 99:1604–1609.

Huang YH, Bergles DE. 2004. Glutamate transporters bring competition to the synapse. Curr Opin Neurobiol 14:346–352.

Huang YH, Dykes-Hoberg M, Tanaka K, Rothstein JD, Bergles DE. 2004. Climbing fiber activation of EAAT4 transporters and kainate receptors in cerebellar Purkinje cells. J Neurosci 24:103–111.

Iino M, Goto K, Kakegawa W, Okado H, Sudo M, Ishiuchi S, Miwa A, Takayasu Y, Saito I, Tsuzuki K, Ozawa S. 2001. Glia-synapse interaction through Ca2+-permeable AMPA receptors in Bergmann glia. Science 292:926–929.

Katagiri H, Tanaka K, Manabe T. 2001. Requirement of appropriate glutamate concentrations in the synaptic cleft for hippocampal LTP induction. Eur J Neurosci 14:547–553.

Kosaka T, Hama K. 1986. Three-dimensional structure of astrocytes in the rat dentate gyrus. J Comp Neurol 249:242–260.

Leary GP, Stone EF, Holley DC, Kavanaugh MP. 2007. The glutamate and chloride permeation pathways are colocalized in individual neuronal glutamate transporter subunits. J Neurosci 27:2938–2942.

Lievens JC, Bernal F, Forni C, Mahy N, Kerkerian-Le Goff L. 2000. Characterization of striatal lesions produced by glutamate uptake alteration: Cell death, reactive gliosis, and changes in GLT1 and GADD45 mRNA expression. Glia 29:222–232.

Lin CL, Bristol LA, Jin L, Dykes-Hoberg M, Crawford T, Clawson L, Rothstein JD. 1998. Aberrant RNA processing in a neurodegenerative disease: The cause for absent EAAT2, a glutamate transporter, in amyotrophic lateral sclerosis. Neuron 20:589–602.

Lissin DV, Gomperts SN, Carroll RC, Christine CW, Kalman D, Kitamura M, Hardy S, Nicoll RA, Malenka RC, von Zastrow M. 1998. Activity differentially regulates the surface expression of synaptic AMPA and NMDA glutamate receptors. Proc Natl Acad Sci USA 95:7097–7102.

Lushnikova I, Skibo G, Muller D, Nikonenko I. 2009. Synaptic potentiation induces increased glial coverage of excitatory synapses in CA1 hippocampus. Hippocampus 19:753–762.

Marie H, Billups D, Bedford FK, Dumoulin A, Goyal RK, Longmore GD, Moss SJ, Attwell D. 2002. The amino terminus of the glial glutamate transporter GLT-1 interacts with the LIM protein Ajuba. Mol Cell Neurosci 19:152–164.

Marrs GS, Green SH, Dailey ME. 2001. Rapid formation and remodeling of postsynaptic densities in developing dendrites. Nat Neurosci 4:1006–1013.

Matsugami TR, Tanemura K, Mieda M, Nakatomi R, Yamada K, Kondo T, Ogawa M, Obata K, Watanabe M, Hashikawa T, Tanaka K. 2006. Indispensability of the glutamate transporters GLAST and GLT1 to brain development. Proc Natl Acad Sci USA 103:12161–12166.

Matute C, Melone M, Vallejo-Illarramendi A, Conti F. 2005. Increased expression of the astrocytic glutamate transporter GLT-1 in the prefrontal cortex of schizophrenics. Glia 49:451–455.

Minelli A, Barbaresi P, Reimer RJ, Edwards RH, Conti F. 2001. The glial glutamate transporter GLT-1 is localized both in the vicinity of and at distance from axon terminals in the rat cerebral cortex. Neuroscience 108:51–59.

Newpher TM, Ehlers MD. 2008. Glutamate receptor dynamics in dendritic microdomains. Neuron 58:472–497.

Nishida H, Okabe S. 2007. Direct astrocytic contacts regulate local maturation of dendritic spines. J Neurosci 27:331–340.

O'Brien RJ, Kamboj S, Ehlers MD, Rosen KR, Fischbach GD, Huganir RL. 1998. Activity-dependent modulation of synaptic AMPA receptor accumulation. Neuron 21:1067–1078.

Oliet SH, Piet R, Poulain DA. 2001. Control of glutamate clearance and synaptic efficacy by glial coverage of neurons. Science 292:923–926.

Perego C, Vanoni C, Bossi M, Massari S, Basudev H, Longhi R, Pietrini G. 2000. The GLT-1 and GLAST glutamate transporters are expressed on morphologically distinct astrocytes and regulated by neuronal activity in primary hippocampal cocultures. J Neurochem 75:1076–1084.

Poitry-Yamate CL, Vutskits L, Rauen T. 2002. Neuronal-induced and glutamate-dependent activation of glial glutamate transporter function. J Neurochem 82:987–997.

Rao VL, Bowen KK, Dempsey RJ. 2001. Transient focal cerebral ischemia down-regulates glutamate transporters GLT-1 and EAAC1 expression in rat brain. Neurochem Res 26:497–502.

Reagan LP, Rosell DR, Wood GE, Spedding M, Muñoz C, Rothstein J, McEwen BS. 2004. Chronic restraint stress up-regulates GLT-1 mRNA and protein expression in the rat hippocampus: Reversal by tianeptine. Proc Natl Acad Sci USA 101:2179–2184.

Regan MR, Huang YH, Kim YS, Dykes-Hoberg MI, Jin L, Watkins AM, Bergles DE, Rothstein JD. 2007. Variations in promoter activity reveal a differential expression and physiology of glutamate transporters by glia in the developing and mature CNS. J Neurosci 27:6607–6619.

Renner M, Specht CG, Triller A. 2008. Molecular dynamics of postsynaptic receptors and scaffold proteins. Curr Opin Neurobiol 18:532–540.

Rothstein JD, Dykes-Hoberg M, Pardo CA, Bristol LA, Jin L, Kuncl RW, Kanai Y, Hediger MA, Wang Y, Schielke JP, Welty DF. 1996. Knockout of glutamate transporters reveals a major role for astroglial transport in excitotoxicity and clearance of glutamate. Neuron 16:675–686.

Rothstein JD, Martin L, Levey AI, Dykes-Hoberg M, Jin L, Wu D, Nash N, Kuncl RW. 1994. Localization of neuronal and glial glutamate transporters. Neuron 13:713–725.

Rothstein JD, Van Kammen M, Levey AI, Martin LJ, Kuncl RW. 1995. Selective loss of glial glutamate transporter GLT-1 in amyotrophic lateral sclerosis. Ann Neurol 38:73–84.

Shibata T, Watanabe M, Tanaka K, Wada K, Inoue Y. 1996. Dynamic changes in expression of glutamate transporter mRNAs in developing brain. Neuroreport 7:705–709.

Spacek J. 1985. Three-dimensional analysis of dendritic spines. III. Glial sheets. Anat Embryol (Berl) 171:245–252.

Stewart MG, Harrison E, Rusakov DA, Richter-Levin G, Maroun M. 2000. Re-structuring of synapses 24 hours after induction of long-term potentiation in the dentate gyrus of the rat hippocampus *in vivo*. Neuroscience 100:221–227.

Stoppini L, Buchs PA, Muller D. 1991. A simple method for organotypic cultures of nervous tissue. J Neurosci Methods 37:173–182.

Sullivan R, Rauen T, Fischer F, Wiessner M, Grewer C, Bicho A, Pow DV. 2004. Cloning, transport properties, and differential localization of two splice variants of GLT-1 in the rat CNS: Implications for CNS glutamate homeostasis. Glia 45:155–169.

Swanson RA, Liu J, Miller JW, Rothstein JD, Farrell K, Stein BA, Longuemare MC. 1997. Neuronal regulation of glutamate transporter subtype expression in astrocytes. J Neurosci 17:932–940.

Tan J, Zelenaia O, Correale D, Rothstein JD, Robinson MB. 1999. Expression of the GLT-1 subtype of Na+-dependent glutamate transporter: Pharmacological characterization and lack of regulation by protein kinase C. J Pharmacol Exp Ther 289:1600–1610.

Tanaka K, Watase K, Manabe T, Yamada K, Watanabe M, Takahashi K, Iwama H, Nishikawa T, Ichihara N, Kikuchi T, Okuyama S, Kawashima N, Hori S, Takimoto M, Wada K. 1997. Epilepsy and exacerbation of brain injury in mice lacking the glutamate transporter GLT-1. Science 276:1699–1702.

Theodosis DT, Poulain DA, Oliet SHR. 2008. Activity-dependent structural and functional plasticity of astrocyte-neuron interactions. Physiol Rev 88:983–1008.

Thévenaz P, Ruttimann UE, Unser M. 1998. A pyramid approach to subpixel registration based on intensity. IEEE Trans Image Process 7:27–41.

Turrigiano G. 2007. Homeostatic signaling: The positive side of negative feedback. Curr Opin Neurobiol 17:318–324.

Turrigiano GG, Leslie KR, Desai NS, Rutherford LC, Nelson SB. 1998. Activity-dependent scaling of quantal amplitude in neocortical neurons. Nature 391:892–896.

Tzingounis AV, Wadiche JI. 2007. Glutamate transporters: Confining runaway excitation by shaping synaptic transmission. Nat Rev Neurosci 8:935–947.

Vanoni C, Massari S, Losa M, Carrega P, Perego C, Conforti L, Pietrini G. 2004. Increased internalisation and degradation of GLT-1 glial glutamate transporter in a cell model for familial amyotrophic lateral sclerosis (ALS). J Cell Sci 117:5417–5426.

Ventura R, Harris KM. 1999. Three-dimensional relationships between hippocampal synapses and astrocytes. J Neurosci 19:6897–6906.

Williams SM, Sullivan RK, Scott HL, Finkelstein DI, Colditz PB, Lingwood BE, Dodd PR, Pow DV. 2005. Glial glutamate transporter expression patterns in brains from multiple mammalian species. Glia 49:520–541.

Witcher MR, Kirov SA, Harris KM. 2007. Plasticity of perisynaptic astroglia during synaptogenesis in the mature rat hippocampus. Glia 55:13–23.

Wong M, Ess KC, Uhlmann EJ, Jansen LA, Li W, Crino PB, Mennerick S, Yamada KA, Gutmann DH. 2003. Impaired glial glutamate transport in a mouse tuberous sclerosis epilepsy model. Ann Neurol 54:251–256.

Yang Y, Gozen O, Watkins A, Lorenzini I, Lepore A, Gao Y, Vidensky S, Brennan J, Poulsen D, Won Park J, Li Jeon N, Robinson MB, Rothstein JD. 2009. Presynaptic regulation of astroglial excitatory neurotransmitter transporter GLT1. Neuron 61:880–894.

Yernool D, Boudker O, Jin Y, Gouaux E. 2004. Structure of a glutamate transporter homologue from Pyrococcus horikoshii. Nature 431:811–818.

Zha X, Green SH, Dailey ME. 2005. Regulation of hippocampal synapse remodeling by epileptiform activity. Mol Cell Neurosci 29:494–506.

Zhou J, Sutherland ML. 2004. Glutamate transporter cluster formation in astrocytic processes regulates glutamate uptake activity. J Neurosci 24:6301–6306.